Egypt. J. Chem. **Vol. 65,** No. SI: 13B pp. 153 - 163 (2022)

Egyptian Journal of Chemistry

http://ejchem.journals.ekb.eg/

Synthesis and Characterization of Feldspar Aluminosilicate Minerals/MCM-48 Composite, Micropore and Mesopore Framework

Ida Ifdaliah Amin[1,2], Abdul Wahid Wahab[*3], Rino R. Mukti[4,5], Paulina Taba[3],

[1] *Doctoral Program of Chemistry, Graduate School University, University of Hasanuddin, South Sulawesi-Indonesia*

[2]*Department of Chemistry, Faculty of Engineering, University of Technology Sulawesi, Makassar City, South Sulawesi-Indonesia*

[3]*Department of Chemistry, Faculty Mathematics and Natural Science, University, University of Hasanuddin, South Sulawesi-Indonesia*

[4] *Division of Inorganic and Physical Chemistry, Institut Teknologi Bandung, Indonesia*

[5]*Research Center for Nanoscience and Nanotechnology, Institut Teknologi Bandung, Indonesia*

Abstract

Natural micromaterials including micro and mesoporous minerals are essential components of sophisticated material cycles and are well known for their biocompatibility and renewability. Meanwhile, feldspar is a rock-forming aluminosilicate mineral that contains alkali metals and is very abundant in nature. The MCM-48 mesoporous material with its 3D pore structure has been widely used in various applications, especially as adsorbents. However, its less hydrothermal nature limits optimal use, consequently, a method such as the combination with micropore feldspar into the mesopore framework is needed to overcome this limitation. Therefore, this study aims to synthesize feldspar mineral composites with MCM-48 by growing the layer on a crystal core using the hydrothermal method for 24 hours at 110°C and calcination for 5 hours at 550°C. The feldspar minerals and aluminosilicate composites formed were characterized by XRD, FTIR, SEM, and BET. The pore size distribution using the DFT method showed a wide mesoporous distribution centered on 23-27Å (from MCM-48) and the presence of low peaks between 6-9Å, thereby indicating a pore distribution identical to the microporous pores of feldspar. The results showed that the MCM-48 modified feldspar composite has been integrated into a single functional unit with new improved physical and chemical properties. Therefore, this composite has the potential to be developed into new materials for multilevel adsorption systems to increase the effectiveness of adsorbents in wastewater containing multi-metals.

Keywords: microporous, mesoporous, alumina silicate, feldspar, MCM-48

1. Introduction

The metal coating, paint, mining, and oil industries have negative impacts such as releasing residual liquid wastes contaminated with heavy metals [1-3]. The presence of heavy metals such as mercury, copper, lead, cadmium, zinc, chromium, nickel, and cobalt in waters potentially causes serious problems for living things, due to the accumulation in the food chain and the entire ecosystems [4-6]. This has prompted the development of smart materials, especially from natural silicate minerals such as feldspar [7], bentonite[8-10], and zeolite [11-13] which have a function as an adsorbent to remove heavy metal waste from the water environment. Natural minerals, especially those from the alumina silicate group, are a common alternative adsorbent since they are abundant in nature and easy to obtain. It is also one of the most abundant mineral groups in the Earth's crust, representing 60% of both the crust and the oceans [14-16]. Meanwhile, feldspar is a crystalline aluminosilicate with the general formula of $M^{1+/}M^{2+}(AlSi)_4O_8$, commonly written as MT_4O_8, where T stands for the element in tetrahedral coordination with oxygen, while M^{1+} and M^{2+} represent the alkali or alkaline earth metals, acting as cation exchangers. The crystal lattice of feldspars has a three-dimensional skeletal structure with cavities made of tetrahedral silica and alumina bonded through

*Corresponding author e-mail: wahidwhb@yahoo.com

Receive Date: 25 January 2022, Revise Date: 19 April 2022, Accept Date: 21 May 2022

DOI: 10.21608/EJCHEM.2022.118194.5325

naturally occurring oxygen atoms. The composition of pure K-feldspar ($KAlSi_3O_8$) is 18 wt% Al_2O_3 and 16.9 wt% K_2O[17]. This structure enables optimal modification to suit different applications. Furthermore, the modification of alumina silicate minerals with MCM-48 mesoporous silica, which has a cubic structure with three-dimensional pore channels allows easier adsorbate diffusion and pore blocking by smaller adsorbates, indicating that it has a lot of potential for a variety of applications, particularly in the adsorption field [18].

The incorporation of mesoporous materials with a core-shell structure is interesting because it allows several components to be integrated into a single functional unit [19-24] with improved physical and new chemical properties [25]. The novelty of this research is that we use the natural mineral Feldspar which is rarely explored from Mesawa District, Indonesia, functionalized with MCM-48 mesoporous material which is expected to produce an advanced material with a core-shell structure that can be applied as a heterogeneous catalyst or selective adsorption of waste. Moreover, the combination of two-pore systems namely alumina silicate and MCM-48 with a micro-mesopore structure can be developed into multiple adsorption systems capable of increasing the effectiveness of adsorbents in wastewater containing several metals. Some of the results previously obtained on the separation of metal ions through the adsorption method are used as a reference in this study [26-29]. This study was conducted to utilize natural resources that are abundantly available for the development of applicative materials. Furthermore, the natural alumina silicate mineral used is applicable as an adsorbent for heavy metal ions in wastewater. Therefore, this study aims to synthesize and characterize natural mineral core-shell composites from MCM-48 for further use in the adsorption field. The characterization of the samples are by X-Ray Diffraction (XRD), Fourier Transform Infrared (FTIR), Scanning Electron Micrographs (SEM), and N_2 adsorption. The XRD spectra use for the identification and phase analysis of materials. The FTIR spectra identify the bonding characteristics, the SEM image to measure pore diameter, and the sample's surface and N_2 adsorption to determine the specific surface area using the Brunauer-Emmett-Teller (BET) method and pore size distribution analysis with the DFT method.

2. **Experimental**

2.1 Material and Reagents

Mesawa crystalline aluminosilicate material details were obtained from Saludengen Village, Mesawa District, Mamasa, West Sulawesi, Indonesia. The reagents used for synthesis were Cetyltrimethyl ammonium bromide (CTAB), Ludox HS-40 (35% w/w SiO_2, 0,4% w/w Na_2O, and 60.1% w/w H_20), Triton X-100 were purchased from Sigma-Aldrich; NaOH p.a (as pellets, E-Merck). Another reagent used in the activation of the raw materials was HCl p.a (E-Merck). A solution of 4M HCL was prepared from the analytical grade of corresponding materials.

2.2. Methods

2.2.1 Mesawa Crystalline Aluminosilicate Material (CM) Preparation

The Mesawa crystalline aluminosilicate material (CM) was cleaned, dried, crushed using a jaw crusher, and then sieved with a 200 mesh sieve. It was further washed with distilled water, stirred for 1 hour at 70˚C, precipitated, and then filtered. Furthermore, the sample was dried in an oven at 105˚C for 1 hour and activated by adding 4 M HCl with a weight ratio of CM to HCl of 1:3. The mixture was stirred for 1 hour at 70˚C and then precipitated, filtered, washed with distilled water until the pH of the filtrate is neutral, and baked for 2 hours at 105˚C. It was then calcined for 5 hours in a furnace at a temperature of 550˚C.

2.2.2. Synthesis of Core-Shell Composite CM/MCM-48

The CM/MCM-48 core-shell composite was synthesized using the hydrothermal synthesis method by modifying a published procedure [27]. 7.15 g of CM material was added to 83.47 g of distilled water, 6.12 g of CTAB, and 1.34 g of Triton. This solution was heated, stirred until homogeneous, and then cooled at room temperature (Solution 1). Furthermore, 14.3 g of Ludox was added to a beaker containing 45.25 g of 1M NaOH, the solution was stirred at 80˚C for 2 hours and then cooled (Solution 2). The two solutions were placed into a polypropylene bottle and stirred vigorously for 15 minutes until homogeneous, then the mixture was heated under static conditions at 100˚C for 24 hours and shaken occasionally. The mixture was cooled to room temperature, then a few drops of acetic acid were added until the pH reached 10. The solution was reheated in the oven at 100˚C for 24 hours, then, it was filtered and washed with distilled water. Moreover, the surfactant was removed by calcination at 550˚C for 5 hours and this composite was coded CM/MCM-48(X), where X is the percentage of the silica-alumina crystals from the total amount of SiO_2 (5, 10, 15, 20, 25%). The schematic illustration for the preparation of core-shell composite CM/MCM-48 is shown in Figure 1.

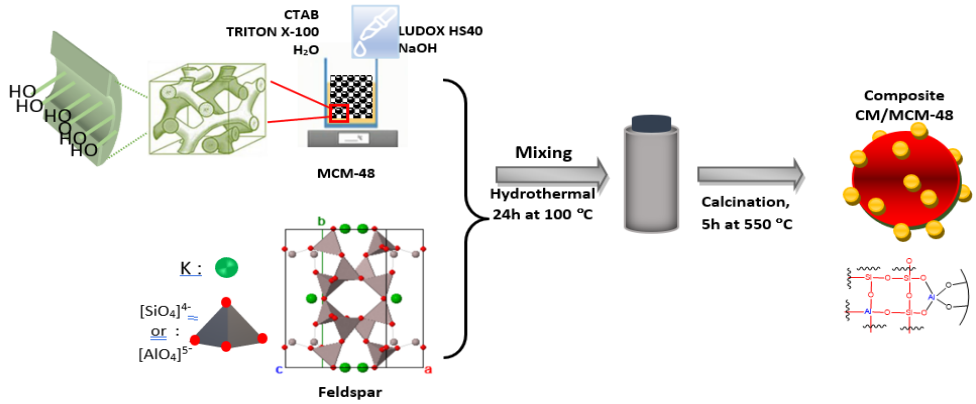

Figure 1. Schematic illustration for the preparation synthesis of core-shell composite CM/MCM-48

2.3. Characterization

XRD patterns were collected using a Shimadzu XRD-700 with Cu Kα radiation. All samples are scanned under the same conditions (2θ = 2-70°), while the scanning electron micrographs (SEM-EDS) were recorded using a JED-2300 analysis station to measure pore diameter and the sample surface. Meanwhile, FT-IR spectroscopy was carried out using Shimadzu 8300 at a wavelength of 4000-250 cm^{-1}. Furthermore, the adsorption-desorption isotherms of nitrogen were obtained at 77.35 K on a Quantrachrome instrument. The liner isotherm was also measured to determine the specific surface area using the BET method, while pore size distribution was assessed with the DFT method.

3. **Results and Discussion**

3.1. Characterization of Mesawa Crystalline Aluminosilicate Material (CM)

The characterization results using XRD showed diffraction patterns of K-feldspar in the form of orthoclase, sanidine, and chabazite phases (Figure 2a). Qualitative analysis was also carried out by comparing the diffraction pattern of the silicate crystals with a standard diffractogram for the orthoclase phase (JCPDS file 86-0439). The result showed the highest peak at d=3.3189 where the value of d is identical for various types of feldspar minerals. When there is a change in the elemental composition, then a shift in the d-value of the mineral is expected. The difference in the XRD pattern of the feldspar mineral group is also due to the composition of the balancing cations namely Na, K, and Ca which are different in each phase. Meanwhile, supporting data analysis of elemental composition in CM material samples using XRF is shown in Table 1.

The results were further supported by the spectral pattern (Figure 2b), where the CM sample exhibits a similar FT-IR spectrum to that of feldspar minerals, as previously reported in [16, 30, 31]. The spectrum shows a peak in the area below 1200 cm^{-1}, due to the intense absorption of Si-O and bending of the OH band, while the peaks around 1091 cm^{-1} indicate asymmetric stretching vibrations of Si-O-Si. Furthermore, the peaks in the area around 578 and 455 cm^{-1} are caused by bending vibrations of Al-O-Si and Si-O-Si, respectively. The result is parallel to the previous report [32]. The vibrational band that shows the characteristics of the K-feldspar was found in the wavenumber around 600 cm^{-1} which is unique for crystal materials [33]

3.2. Composite CM/MCM-48

The XRD patterns of the CM/MCM-48 composite with the percentage addition of CM material weight to the total amount of different SiO_2 namely 5, 10, 15, 20, and 25% by weight with a hydrothermal time of 24 hours is shown in Figure 3. The characteristics of the mesopore mineral are demonstrated in the XRD pattern for the low-angle area (Figure 3A). There are 3 different diffraction planes at angles of 2θ = 2.5° (211), 3.2° (320), and 4.5° (420) indicating a good structural arrangement in the la3d cubic crystallographic space group appropriate to the pattern reported for the pure MCM-48 mesopore silica material. The addition of 5% (3A-a) and 10% 32A-b) did not appropriately show the peak characteristic of the cubic phase as the broad peak in the 2θ = 4,5° region was not clearly shown. Meanwhile, the addition of 20 and 25% CM material (figure 3A d, e) showed a well resolved characteristic peak according to the silica phase of MCM-48 with a sharp peak at 2θ = 2.5°; 3.2°; and 4.5° especially at 25% increments. However, the peak intensity seemed to decrease with the increase in the mineral, especially at the addition of 15, 20, and 25%. The decrease is caused by the grafting of silanol groups in the mesopore framework, this implies that the percentage of CM material addition affects the formation of MCM-48. Nevertheless, it was observed that in the addition from 5%-25%, all composites appropriately exhibited the mesopore and mineral structure. The XRD data comparison shows that the composite with the addition of 25% produced the best MCM-48 structure and the feldspar minerals compared to the others.

Table 1. Elemental composition of Mesawa crystalline aluminosilicate material (CM)

Compound	SiO_2	K_2O	Fe_2O_3	CaO	Al_2O_3
w/w (%)	53.01	6.86	2.59	1.53	15.73

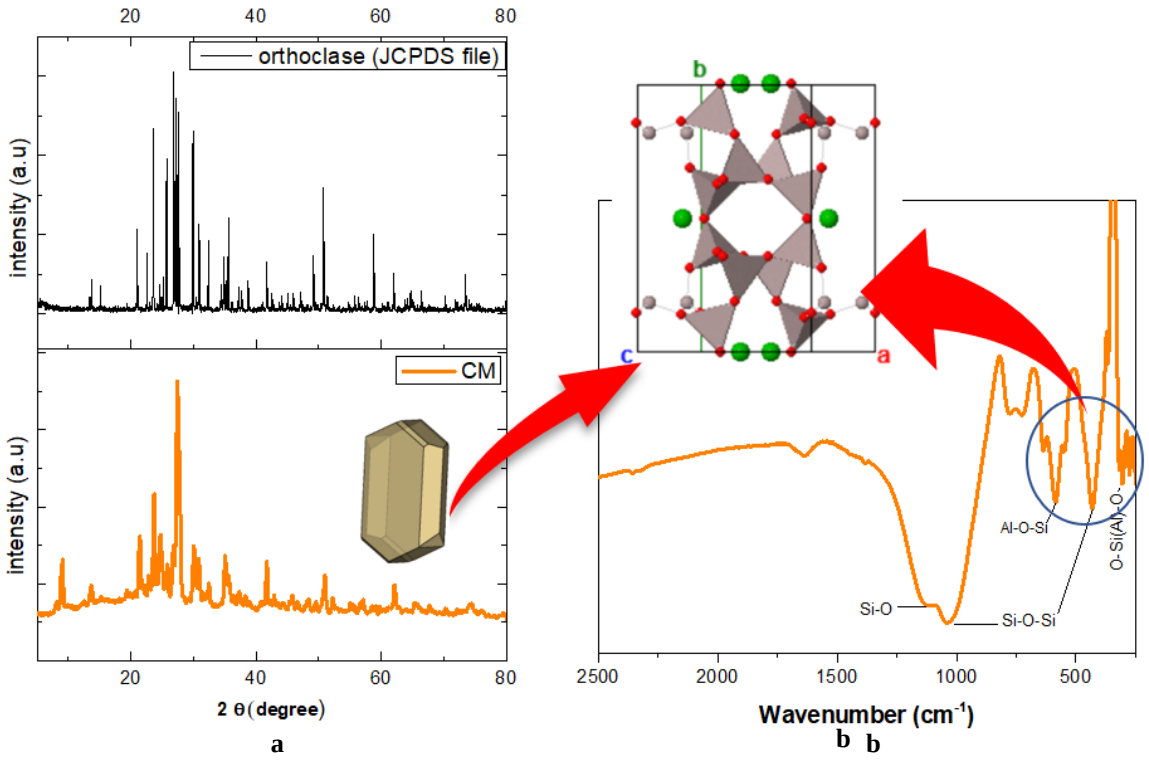

Figure 2. XRD diffraction pattern of CM material and Orthoclase phase (a), FTIR spectrum of CM material (b).

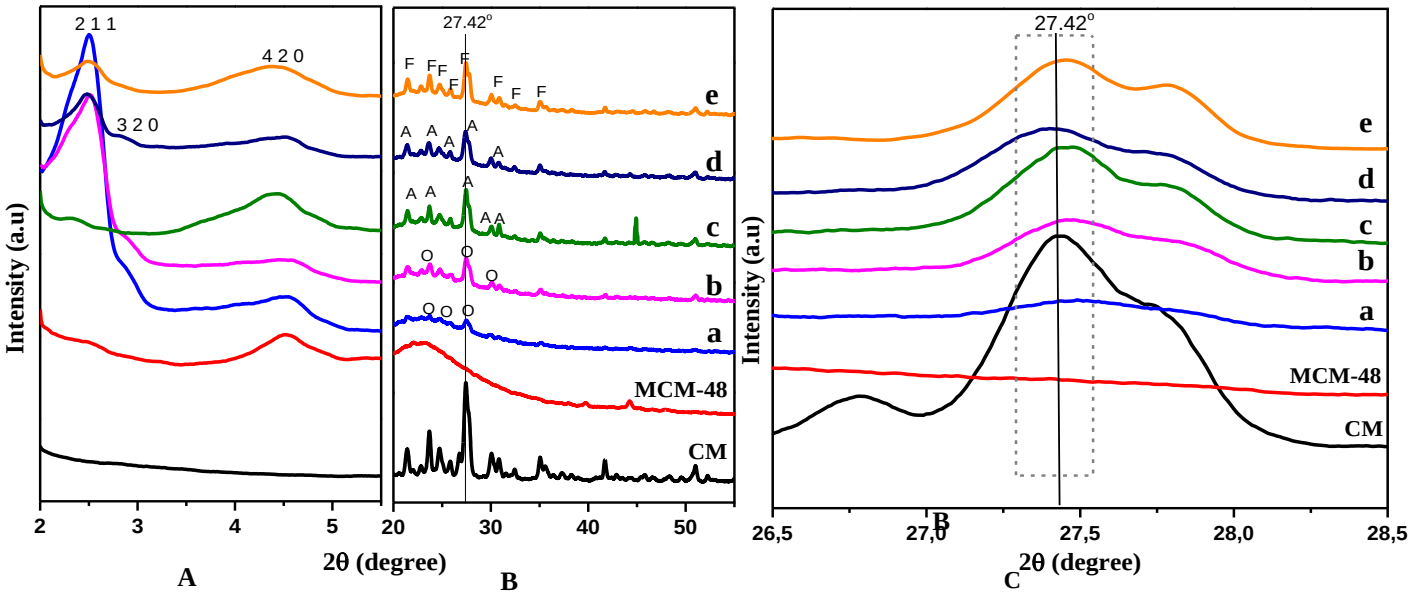

Figure 3. XRD diffraction pattern for composites in low angel (A) and high angel (B) regions, (C) XRD pattern magnification image at the highest peak 2θ=27,42°, where (a) for composite CM/MCM-48(5%), (b) composite CM/MCM-48(10%), (c) CM/MCM-48(15%), (d) CM/MCM-48(20%), and (e) composite CM/MCM-48(25%); A=Anorthoclase, F= Feldspar, O=Orthoclase;

In the high angle region, although all composite samples show a consistent set of phases, a small difference in relative intensity was observed (Figure. 3B). Changes in the characteristic peak of orthoclase as the main phase in the CM samples were observed in all the CM/MCM-48 composites (area 2θ= 27.29°-27.51°) which is appropriate with the characteristics of anorthoclase K-feldspar. The peak intensity obtained with the 5 and 10% addition was still relatively weak compared to the 15 and 20% addition. Subsequently, changes in the structure of orthoclase to anorthoclase in the composite sample were associated with variations in the Na or K sites, where the Na ion which predominated moved towards the Feldspar framework. Therefore, the material structure changed from orthoclase ($K(AlSi_3O_8)$) to anorthoclase (Na, K ($AlSi_3O_8$)) as shown in Figure 3B (a-d). This implies that the thermal changes for ion exchange occurred in the composite to form a new mineral crystalline phase. The detail of the peak shift in the composite sample is shown in Figure 3C. Meanwhile, this phenomenon has previously been described in the JCPDS file which reported a shift in the highest peak from the orthoclase (JCPDS file 86-0439) phase in the fraction plane from d= 3.3189Å to anorthoclase (JCPDS file 76-0803) with the highest peak at d= 3.2410Å [34]. The phase change at the addition of 25% is probably due to the higher percentage of CM crystals, where the alumina silicate molar ratio is closer to the ideal feldspar ratio is between 3:1 to 1:1[35].

The XRD pattern of the CM/MCM-48 composite in the high angle region (Figure. 3B) shows that the characteristic peak of the CM material (feldspar) is covered by intense and wide peaks around 2θ= 23-25°. This broad peak is appropriate with the amorphous SiO_2 forming the MCM-48 wall, indicating that the CM material structure is present in the composite sample. Moreover, this phenomenon is attributed to the formation of the desired mesostructure after the changes in the mineral structure and further recrystallization under strongly alkaline conditions. The presence of the CM material structure and the MCM-48 mesopore material in the composite is also supported by data from the FT-IR spectra.

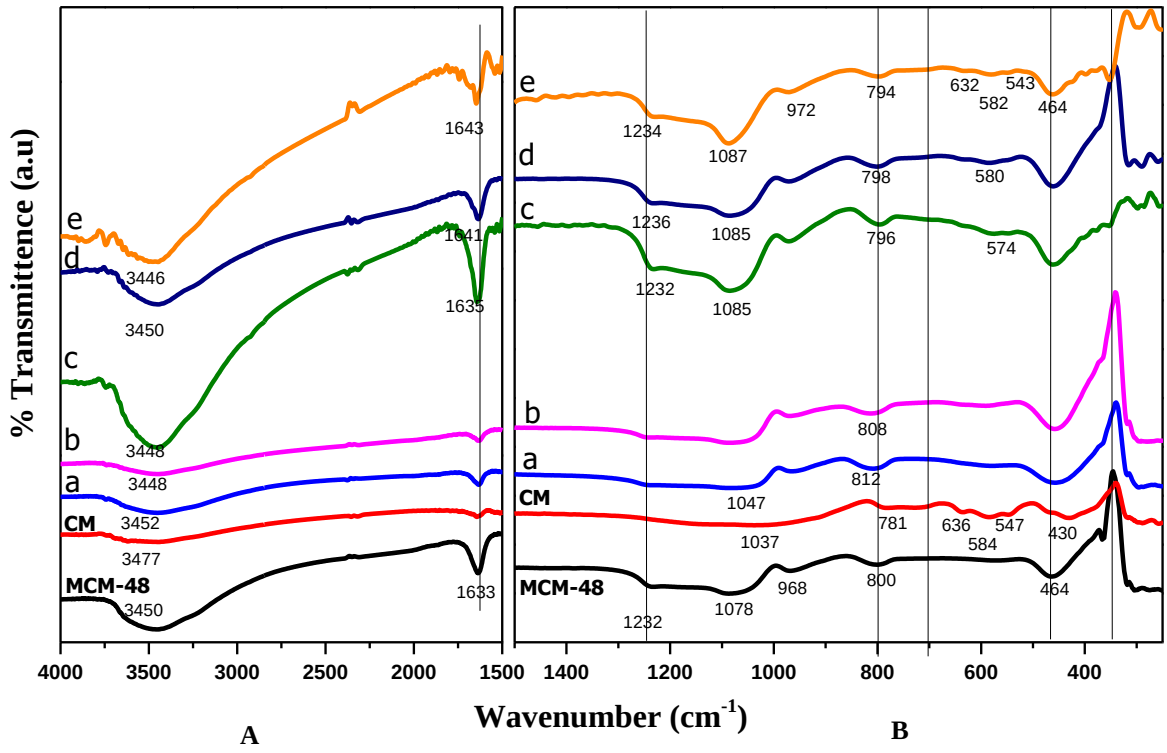

Figure 4. FTIR spectrum at wavenumber 4000-1500 cm^{-1} (A) and at wavenumber 1400-350 cm^{-1} (B) for (a) composite CM/MCM-48 (5%), (b) composite CM/MCM-48 (10%), (c) composite CM/MCM-48 (15%), (d) composite CM/MCM-48 (20%), and (e) composite CM/MCM-48 (25%)

Figure 4 shows the infrared spectrum of CM/MCM48 composites with various percentages of CM material. The main peak characteristic of the vibrational mode was found between 1078-1089 cm^{-1} while the infrared spectrum shows a wide peak in the wavenumber region of 3442-3464 cm^{-1} as demonstrated by the 15, 20, and 25% composite samples (Figure 4A c-e). Meanwhile, in the 5 and 10% composite samples, the peak intensity appeared weak with -OH stretching supported by bending vibrations

in the absorption band in the region of 1633-1641 cm^{-1} for the hydroxyl group (from silanol) and water which is physically adsorbed by MCM-48 (Figure 4A a-b). Adsorption at 1230 cm^{-1} regions is assigned to the asymmetric stretching and bonding of ≡Si-O-Si≡ of the MCM-48. The strong absorption band peaks at 1085 cm^{-1} (15%), 1085 cm^{-1} (20%), and 1087 cm^{-1} (25%) are asymmetric stretching vibrations associated with T-O-T (T=Si/Al). In contrast, the weak absorption band in the 968-972 cm^{-1} wavenumber region is the Si-O stretching vibration of Si-OH (Figure 4B c-e). Meanwhile, the symmetrical stretching vibration of Si-O-Si from the silicate lattice is shown in the absorption band at 812-781 cm^{-1} and supported by Si-O-Si bending vibrations at 457 and 464 cm^{-1}. Absorption bands in 729 and 623 cm^{-1} regions indicate tetrahedron vibrations, while 578, 592, 574, 580, and 582 cm^{-1} regions indicate O-Si/Al-O bending vibrations in CM micropores[30]. Table 2 represents the band assignments of CM/MCM48 composites. This peak appeared along with the increase in the amount of CM material in the composite. The absorption band in the area of 600 - 500 cm^{-1} is a characteristic of CM and represents a unique region for crystalline materials. This pattern indicates that Mesawa alumina silicate crystals are formed throughout the MCM-48 mesopore matrix.

Table 2. Present band assignments of CM/MCM48 composites

Assignments	CM/MCM-48 composites					Ref.
	5%	10%	15%	20%	25%	
	Wavenumber (cm^{-1})					
-Si-O-Si	457	459	460	460	464	[33]
-O-Si(Al)-O	578	592	574	580	582	[33]
-Si-O-Si	812	808	796	798	794	[30]
-Si-O-	1083	1085	1085	1085	1087	[36]
≡Si-O-Si≡	-	1240*	1232	1236	1234	[36]
≡Si-OH bending	1631*	1633*	1635	1641	1643	[36]
-OH	3452*	3448*	3464	3450	3442	[36]

Note: *= low intensity

The SEM image results show the shape of the CM material, which is described as crystalline feldspar (Figure 4a), the shape of the MCM-48 mesoporous material, which is described as a sponge (Figure 5b), and the shape of the CM/MCM-48 composite (Figure 5c, d, e). The presence of CM material attached to the surface of MCM-48 indicates that the synthesis of the CM/MCM-48 composite was successful. The CM core is still visible with the addition of 5% CM material, but with the addition of 15% and 25% CM material, it is clear that the CM material has been covered by MCM-48. The presence of crystals in the CM/MCM-48 composite is strongly supported by the combination of XRD and SEM-EDX results. Figure 4f shows a schematic representation of the synthesis process. The previously added CM material served as seed material, and MCM-48 overgrew on the CM material's surfaces.

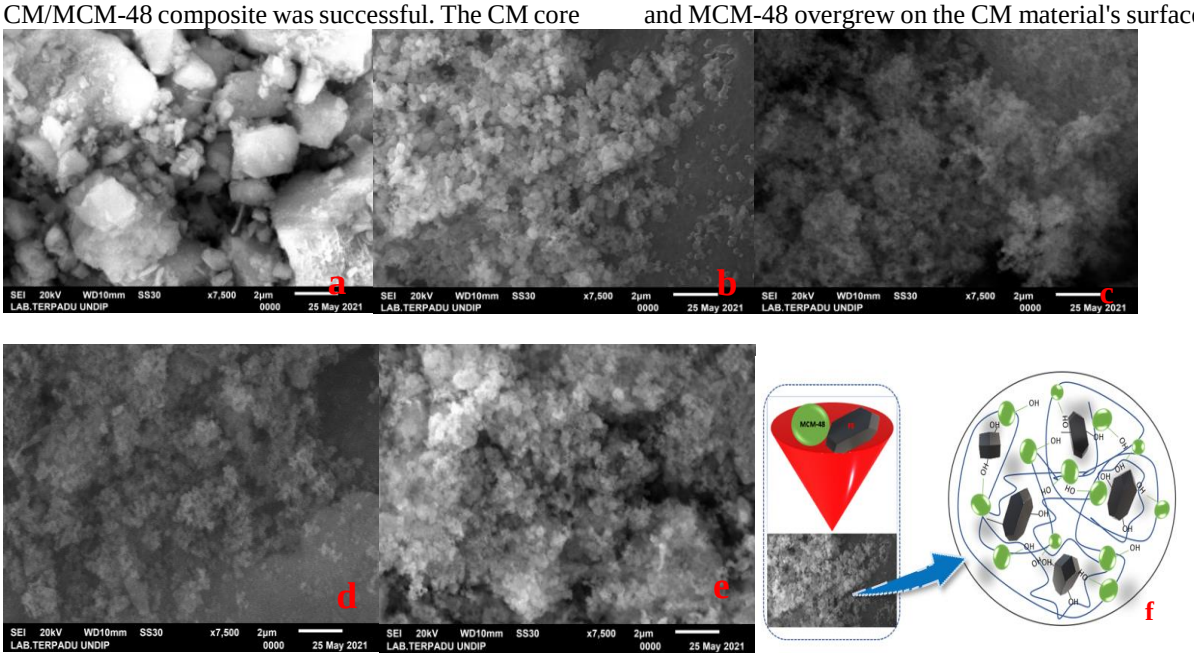

Figure 5. SEM images for (a) CM, (b) MCM-48, (c) composite CM/MCM-48 (5%), (d) composite CM/MCM-48 (15%), (e) composite CM/MCM-48 (25%), and (f) Schematic illustration interaction within CM/MCM-48

3.3. Pore Structure of Composite

The pore properties of MCM-48, CM, and CM/MCM-48 composite materials are indicated by the measurement of N_2 absorption. The N_2 desorption-adsorption isotherm for feldspar materials showed a typical type I isotherm which is indicative of micropores, while MCM-48 shows a type IV isotherm typical for mesopore materials (Figure 6A). The absence of hysteresis between the relative pressures of P/Po 0.1 – 0.2 shows the smallest indication of reversible adsorption in the mesopores. Meanwhile, a sharp increase in the relative P/Po pressure of 0.8 – 1 indicates a hysteresis loop associated with the space between particles called texture porosity. In this study, the mesostructures formation was observed in all samples along with an isotherm similar to well-formed MCM-48 silica (Figure 6B).

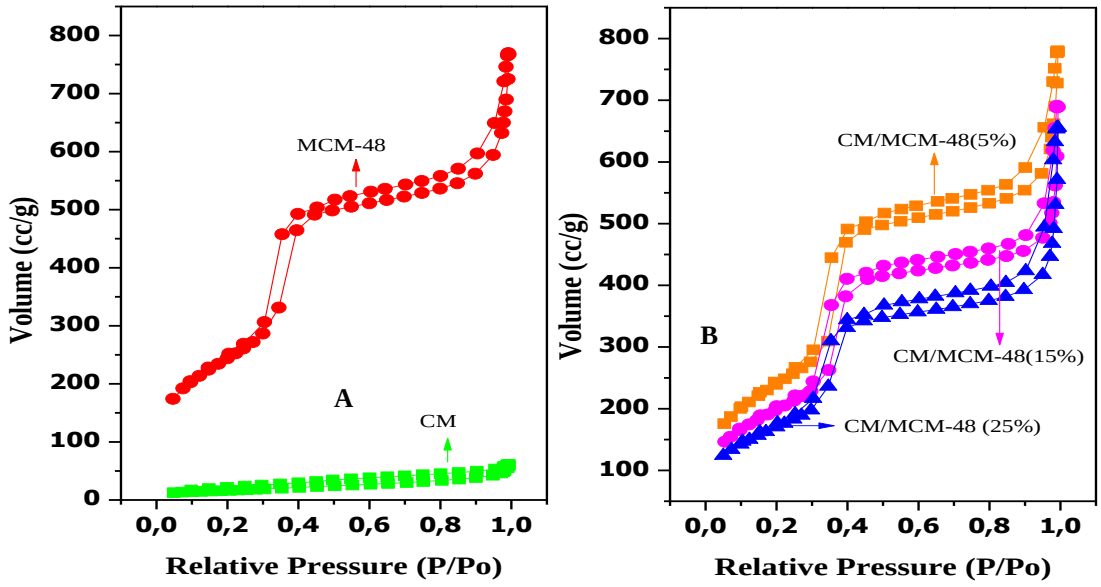

Figure 6. N_2 adsorption-desorption isotherms at 77,35 K

All composite isotherms displayed a marked condensation step with a sharp slope in the P/Po = 0.3-0.4 relative pressure region followed by a wide hysteresis loop. This indicates a wide distribution of mesopore sizes. In general, the uptake of N_2 at this relative pressure decreased with the increasing amount of CM material added. This shows that the proportion of CM material affects the isotherm shape and N_2 absorption. Furthermore, the pore size distribution using the DFT method shows a wide mesoporous distribution centered on 23-27Å (from MCM-48) and the presence of low peaks between 6-9Å, thereby indicating a pore distribution identical to the microporous pores of feldspar (Figure 7). Therefore, the size of the micro peaks was smaller than the meso-peaks because the amount of MCM-48 used was higher than CM. This shows that the synthesized composite has several micropores and mesopores.

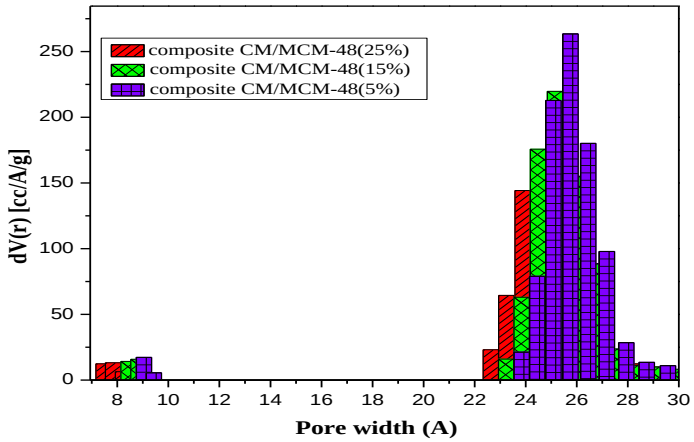

Figure 7. PSDs calculated by DFT method for CM/MCM-48(5%), CM/MCM-48(15%), and CM/MCM-48(25%) composite.

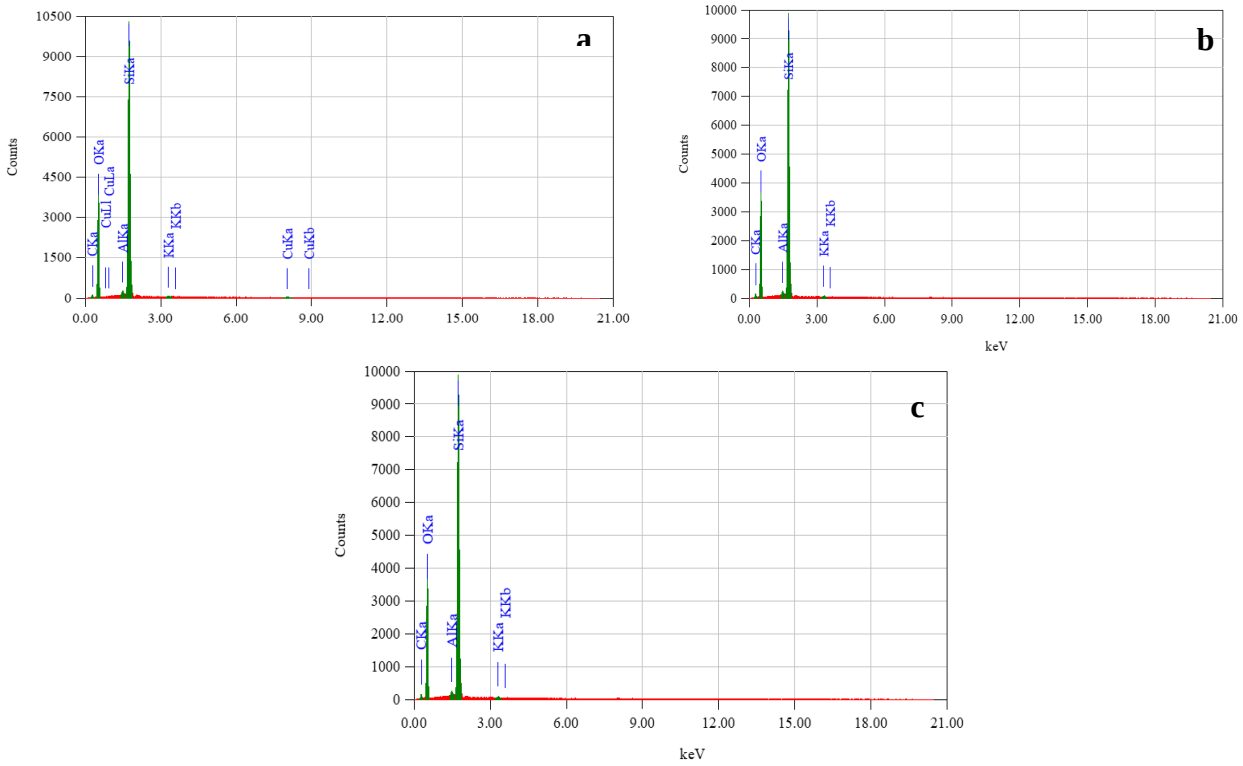

Figure 8. EDS spectra and microchemical point analyses of the composite: a. CM/MCM-48(5%), b. CM/MCM-48(15%), and c. CM/MCM-48(25%).

The CM material acts as the core and supports the crystallization of MCM-48 shown by the SEM images in Figure 4, while the pore texture parameters derived from the adsorption isotherm are presented in Table 3. Furthermore, the specific surface area was measured using the Brunauer-Emmett-Teller (BET) method. The adsorption-desorption analysis of N_2 showed that the pore surface area of the composite is between the CM and MCM-48 mesoporous material. Based on the results, the surface area decreased with the addition of CM material at intervals of 870-620 m^2g^{-1}. This is due to the contribution of mesopores and micropores, while the MCM-48 pore closure was caused by the added feldspar material as demonstrated by the XRD data which shows a decrease in intensity for composite materials [37].

Table 3. Porous texture parameter was obtained from the N_2 adsorption isotherms at 77,35 K for CM/MCM-48(5%), CM/MCM-48(15%), and CM/MCM-48(25%) composite.

	S BET (m^2g^{-1})	Micropore volume (cm^3g^{-1})	Pore radius Dv(r) (nm)	Pore volume (cm^3g^{-1})
CM	58	0.02	1.53	0.08
MCM-48	893	0.25	1.69	0.98
CM-MCM-48(5%)	870	0.25	1.70	0.99
CM-MCM-48(15%)	719	0.20	1.71	0.81
CM-MCM-48(25%)	620	0.17	1.69	0.77

It is well known that strong alkaline hydrothermal treatment promotes the removal of silicon atoms from the feldspar framework, this is relevant to the EDS data that was carried out after treatment of each composite (Figure 8). This selective extraction causes the collapse of adjacent micropores, resulting in mesopores measuring about 23–27Å. Furthermore, when alkaline treatment is carried out in the presence of organic cations, the dissolved aluminosilicate secondary building units can again condense around the CTAB micelles, which function as pore growth drivers. Therefore, the emergence of new maxima in PSD for composite samples (Figure. 7) indicates that 24 h treatment will establish mesoporosity through the process mentioned above. On the other hand, dissolved silica units can easily

settle on the feldspar surface or enter the pores, causing pore clogging and pore size reduction, respectively [26, 27]. The surface area decreased substantially (from 870 to 620 m^2g^{-1}, see Table 3). A decrease in the surface area was observed during 12 hours of treatment, silica deposition at the entrance of the feldspar micropores was manifested by a moderate decrease in pore size during 24 hours of hydrothermal treatment.

Y Zeolite/MCM-48 has been successfully synthesized, according to prior research [18], and this composite material exhibited the mesoporous and microporous features of MCM-48 and zeolite Y, with the primary pore diameter of 3,2 nm. In comparison to MCM-48, this composite had thicker pore walls and higher acidity. In addition, the core-shell Y zeolite/MCM-48 composite had micropore and mesopore volumes ranging between 0.15-0.30 and 0.30-0.51 cm^3g^{-1}, respectively [37]. The data generated from the characteristics of the CM/MCM-48 composite is not considerably different from the previous literature, so it is expected that the CM/MCM-48 composite has capabilities comparable to other composites, based on the literature. As a result, this substance is predicted to be useful in reclaiming areas that have been contaminated with many elements.

4. **Conclusion**

The core/shell composite CM/MCM-48 with a micropore-mesopore framework was successfully synthesized from the MCM-48 mesopore membrane with the addition of CM material. It has been identified as a K-Feldspar mineral as a source of silica and aluminum with an inner micropore framework under hydrothermal conditions. The composite structure was appropriately obtained with high thermal stability and calcination up to 550°C. The surface area decreased with the addition of feldspar material at intervals of 870-620 m^2g^{-1}. The pore size distribution using the DFT method shows a wide mesoporous distribution centered on 23-27 Å and the presence of low peaks between 6-9 Å, thereby indicating a pore distribution identical to the microporous pores of feldspar. Therefore, the exposed surface of the composite provides a better active site, making it a possibility for increased adsorption/desorption of heavy metals in water.

5. **Conflict of Interest** There is no conflict of interest related to this research.

6. Acknowledgments

The author is grateful to the Directorate General of DIKTI-Kemendiknas through the Hasanuddin University BPPDN in 2019/2020 and the PDD Grant in 2020/2021 with contract number: 7/E1/KP.PTNBH/2021 March 8, 2021; No: 8046/UN4.1.2.3/PL.02.00/2021 March 22, 2021, and No: 761/UN4.22/PT.01.03.2021 March 26, 2021.

7. References

[1] S.S. Obaid, D.K. Gaikwad, M.I. Sayyed, K. Al-Rashdi, P.P. Pawar, Heavy metal ions removal from waste water bythe natural zeolites, Materials Today: Proceedings 5(9) (2018) 17930-17934.

[2] Y.A.B. Neolaka, G. Supriyanto, H.S. Kusuma, Adsorption performance of Cr(VI)-imprinted poly(4-VP-co-MMA) supported on activated Indonesia (Ende-Flores) natural zeolite structure for Cr(VI) removal from aqueous solution, Journal of Environmental Chemical Engineering 6(2) (2018) 3436-3443.

[3] X. Lu, F. Wang, X.-y. Li, K. Shih, E.Y. Zeng, Adsorption and Thermal Stabilization of Pb2+ and Cu2+ by Zeolite, Industrial & Engineering Chemistry Research 55(32) (2016) 8767-8773.

[4] M. Naushad, Z. Abdullah Alothman, M. Rabiul Awual, S.M. Alfadul, T. Ahamad, Adsorption of rose Bengal dye from aqueous solution by amberlite Ira-938 resin: kinetics, isotherms, and thermodynamic studies, Desalination and Water Treatment 57(29) (2015) 13527-13533.

[5] A.B. Albadarin, M.N. Collins, M. Naushad, S. Shirazian, G. Walker, C. Mangwandi, Activated lignin-chitosan extruded blends for efficient adsorption of methylene blue, Chemical Engineering Journal 307 (2017) 264-272.

[6] T.P. Fato, D.W. Li, L.J. Zhao, K. Qiu, Y.T. Long, Simultaneous Removal of Multiple Heavy Metal Ions from River Water Using Ultrafine Mesoporous Magnetite Nanoparticles, ACS Omega 4(4) (2019) 7543-7549.

[7] M. Yazdani, N. Mohammad Mahmoodi, M. Arami, H. Bahrami, Isotherm, Kinetic, and Thermodynamic of Cationic Dye Removal from Binary System by Feldspar, Separation Science and Technology 47(11) (2012) 1660-1672.

[8] B. Anna, M. Kleopas, S. Constantine, F. Anestis, B. Maria, Adsorption of Cd(II), Cu(II), Ni(II) and Pb(II) onto natural bentonite: study in mono- and multi-metal systems, Environmental Earth Sciences 73(9) (2014) 5435-5444.

[9] P. Kumararaja, K.M. Manjaiah, S.C. Datta, B. Sarkar, Remediation of metal contaminated soil by aluminium pillared bentonite: Synthesis, characterisation, equilibrium study and plant growth experiment, Applied Clay Science 137 (2017) 115-122.

[10] Y. Sun, Y. Li, Y. Xu, X. Liang, L. Wang, In situ stabilization remediation of cadmium (Cd) and lead (Pb) co-contaminated paddy soil using bentonite, Applied Clay Science 105-106 (2015) 200-206.

[11] M. Hong, L. Yu, Y. Wang, J. Zhang, Z. Chen, L. Dong, Q. Zan, R. Li, Heavy metal adsorption with

zeolites: The role of hierarchical pore architecture, Chemical Engineering Journal 359 (2019) 363-372.
[12] T.P. Belova, Adsorption of heavy metal ions (Cu(2+), Ni(2+), Co(2+) and Fe(2+)) from aqueous solutions by natural zeolite, Heliyon 5(9) (2019) e02320.
[13] L. Darmayanti, G.T.M. Kadja, S. Notodarmojo, E. Damanhuri, R.R. Mukti, Structural alteration within fly ash-based geopolymers governing the adsorption of Cu(2+) from aqueous environment: Effect of alkali activation, J Hazard Mater 377 (2019) 305-314.
[14] T. Skorina, A. Allanore, Aqueous alteration of potassium-bearing aluminosilicate minerals: from mechanism to processing, Green Chemistry 17(4) (2015) 2123-2136.
[15] F.K. Crundwell, The mechanism of dissolution of the feldspars: Part II dissolution at conditions close to equilibrium, Hydrometallurgy 151 (2015) 163-171.
[16] J. Yuan, J. Yang, H. Ma, S. Su, Q. Chang, S. Komarneni, Hydrothermal synthesis of nano-kaolinite from K-feldspar, Ceramics International 44(13) (2018) 15611-15617.
[17] H. Salimkhani, T. Joodi, A. Bordbar-Khiabani, A. Motei Dizaji, B. Abdolalipour, A. Azizi, Surface and structure characteristics of commercial K-Feldspar powders: Effects of temperature and leaching media, Chinese Journal of Chemical Engineering 28(1) (2020) 307-317.
[18] Y. Zhang, Y. Liu, Y. Li, Synthesis and characteristics of Y-zeolite/MCM-48 biporous molecular sieve, Applied Catalysis A: General 345(1) (2008) 73-79.
[19] A. Azhati, S. Xie, W. Wang, A.A. Elzatahry, Y. Yan, J. Zhou, D. Al-Dhayan, Y. Zhang, Y. Tang, D. Zhao, Ordered, Highly Zeolitized Mesoporous Aluminosilicates Produced by a Gradient Acidic Assembly Growth Strategy in a Mixed Template System, Chemistry of Materials 28(13) (2016) 4859-4866.
[20] P.S. Lee, D.-Y. Hong, G.-Y. Cha, H. An, S.-Y. Moon, M. Seong, B.-J. Chang, J.S. Lee, J.-H. Kim, Mixed matrix membranes incorporated with three-dimensionally ordered mesopore imprinted (3DOm-i) zeolite, Separation and Purification Technology 210 (2019) 29-37.
[21] N.T. Tran, J. Kim, M.R. Othman, Microporous ZIF-8 and ZIF-67 membranes grown on mesoporous alumina substrate for selective propylene transport, Separation and Purification Technology 233 (2020).
[22] W. Li, D. Zhao, Extension of the Stober method to construct mesoporous SiO2 and TiO2 shells for uniform multifunctional core-shell structures, Adv Mater 25(1) (2013) 142-9.
[23] C. Dai, A. Zhang, M. Liu, L. Gu, X. Guo, C. Song, Hollow Alveolus-Like Nanovesicle Assembly with Metal-Encapsulated Hollow Zeolite Nanocrystals, ACS Nano 10(8) (2016) 7401-8.
[24] X.-L. Luo, F. Pei, W. Wang, H.-m. Qian, K.-K. Miao, Z. Pan, Y.-S. Chen, G.-D. Feng, Microwave synthesis of hierarchical porous materials with various structures by controllable desilication and recrystallization, Microporous and Mesoporous Materials 262 (2018) 148-153.
[25] F. Fu, L. Xie, B. Tang, Q. Wang, S. Jiang, Application of a novel strategy—Advanced Fenton-chemical precipitation to the treatment of strong stability chelated heavy metal containing wastewater, Chemical Engineering Journal 189-190 (2012) 283-287.
[26] C. Yang, X. Meng, D. Yi, Z. Ma, N. Liu, L. Shi, Core–Shell Zeolite Composite with Silicalite-1/NaY Structure for the Adsorption Desulfurization of Dimethyl Disulfide from Methyl tert-Butyl Ether, Industrial & Engineering Chemistry Research 57(48) (2018) 16358-16366.
[27] S. Sohrabnezhad, N. Karkoudi, A. Asadollahi, Core–shell composite of mordenite zeolite@MCM-41mesoporous: Synthesis, characterization and application in photocatalytic activity, Colloids and Surfaces A: Physicochemical and Engineering Aspects 520 (2017) 17-25.
[28] H. Yu, Y. Lv, K. Ma, C. Wang, Z. Xue, Y. Zhao, Y. Deng, Y. Dai, D. Zhao, Synthesis of core-shell structured zeolite-A@mesoporous silica composites for butyraldehyde adsorption, J Colloid Interface Sci 428 (2014) 251-6.
[29] X. Luo, J. Guo, P. Chang, H. Qian, F. Pei, W. Wang, K. Miao, S. Guo, G. Feng, ZSM-5@MCM-41 composite porous materials with a core-shell structure: Adjustment of mesoporous orientation basing on interfacial electrostatic interactions and their application in selective aromatics transport, Separation and Purification Technology 239 (2020).
[30] L. Xu, J. Tian, H. Wu, W. Deng, Y. Yang, W. Sun, Z. Gao, Y. Hu, New insights into the oleate flotation response of feldspar particles of different sizes: Anisotropic adsorption model, J Colloid Interface Sci 505 (2017) 500-508.
[31] J. Yuan, J. Yang, H. Ma, C. Liu, C. Zhao, Hydrothermal synthesis of analcime and hydroxycancrinite from K-feldspar in Na2SiO3solution: characterization and reaction mechanism, RSC Advances 6(59) (2016) 54503-54509.
[32] M. Yazdani, T. Tuutijärvi, A. Bhatnagar, R. Vahala, Adsorptive removal of arsenic(V) from aqueous phase by feldspars: Kinetics, mechanism,

and thermodynamic aspects of adsorption, Journal of Molecular Liquids 214 (2016) 149-156.
[33] D. B. Ghale, N. B. Bohara, N. Duwal, J. Bhattarai, Investigation on the Mineralogical Phase of Ancient Brick Samples of Kathmandu Valley (Nepal) Using Xrd and Ftir Analysis, Rasayan Journal of Chemistry 12(02) (2019) 402-408.
[34] L.C. Harnett, L.J. Gardner, S.-K. Sun, C. Mann, N.C. Hyatt, Reactive spark plasma sintering of Cs-exchanged chabazite: characterisation and durability assessment for Fukushima Daiichi NPP clean-up, Journal of Nuclear Science and Technology 56(9-10) (2019) 891-901.
[35] B. Mason, C.B. Moore, Principles of geochemistry, (1985).
[36] M. Bandyopadhyay, N. Tsunoji, T. Sano, Mesoporous MCM-48 Immobilized with Aminopropyltriethoxysilane: A Potential Catalyst for Transesterification of Triacetin, Catalysis Letters 147(4) (2017) 1040-1050.
[37] M. Enterría, F. Suárez-García, A. Martínez-Alonso, J.M.D. Tascón, Preparation of hierarchical micro-mesoporous aluminosilicate composites by simple Y zeolite/MCM-48 silica assembly, Journal of Alloys and Compounds 583 (2014) 60-69.